

FINAL TECHNICAL REPORT:
Award Number G12AP20030
Three Dimensional Models of Episodic Tremor and Slip in
Cascadia

April 7, 2014

Paul Segall
(650-723-7241, segall@stanford.edu)
Geophysics Department
Stanford University
Stanford, CA 94305-2215

Award Dates: 1/2012–12/2013

Abstract

We continue development of physical models of slow slip events based on dilatant strengthening. We further compare model predictions with observations from the Cascade subduction zone. Slow slip events (SSE) in many subduction zones incrementally stress the adjacent locked megathrust, suggesting that they could potentially either trigger or evolve into damaging earthquakes. We explored this with 2D quasi-dynamic simulations with rate-state friction, dilatancy, and coupled 1D pore-fluid and heat transport. Steady-state weakening friction allows transient slip to nucleate, but is inhibited by dilatant strengthening and destabilized by thermal pressurization. SSE spontaneously nucleate in Low Effective-Stress Velocity-Weakening (LESVW) regions. If the dimension of the LESVW is relatively small the SSE are trapped at its updip end, imparting a strong stress concentration in the locked zone. After several centuries SSE penetrate into the region of higher effective stress, where thermal pressurization eventually leads to dynamic rupture. For larger LESVW regions SSE tend to increase in length with time; ultimately higher slip speeds enhance thermal weakening, leading to dynamic instability within the SSE zone. In both cases the onset of the ultimate SSE is essentially indistinguishable from preceding events.

We also compared predictions of models with dilatancy to models in which the friction coefficient transitions from weakening to strengthening at an intermediate slip speed. The two classes of models can be made rather similar, although dilatancy models exhibit less regularity as the length of the slipping zone becomes large relative to characteristic frictional stability length scales. Importantly, both classes of models predict that slip in the ETS zone lags plate motion, and that dynamic events rupture into the ETS zone.

The predictions of the dilatancy-based model are compared with GPS observations, both during and between SSE events. The fit to average SSE displacements using the inferred distributions of frictional properties and effective normal stress is remarkably good, suggesting

that the the low effective stress – velocity weakening region is in roughly the correct depth range. The fit to the inter-ETS data is not as good, and seems to require modest inter-seismic creep (≤ 12 mm/yr) above the ETS zone, at depths of $\lesssim 20$ km. We explored whether or not viscoelastic effects could help explain the “gap” between the down-dip limit of inter-seismic locking and the top of the ETS zone. We find that viscoelastic effects can improve the fit to horizontal GPS velocities but not the vertical rates from leveling and tide-gauge data.

We have made great progress on developing numerical methods to accelerate 3D simulations of fault behavior. We developed Hierarchical-matrix (H-matrix) compression software library `hmmvp`, that allows computation of Boundary Element calculations in $O(n \log n)$ time, rather than $O(n^2)$ time for uncompressed matrix vector products. This software is open source and available at <https://pangea.stanford.edu/research/CDFM/software/index.html>.

1 Report

In this report we present results to a number of questions raised in the proposal:

How does the model behavior depend on depth-dependent frictional properties and effective stress, including the effects of finite thickness shear zones?

We published two papers on this topic in 2012. They are briefly reviewed here:

Segall, P. and A. M. Bradley, The role of thermal pressurization and dilatancy in controlling the rate of fault slip, Journal of Applied Mechanics, 79, 2012, doi:10.1115/1.4005896.

We developed two-dimensional quasi-dynamic simulations that include rate-state friction, dilatancy, and heat and pore fluid flow normal to the fault. We found that at lower background effective normal stress slow slip events occur spontaneously, whereas at higher effective normal stress slip is inertially limited. At intermediate values dynamic events are followed by quiescent periods, and then long durations of repeating slow slip events. In these cases, accelerating slow events ultimately nucleate dynamic rupture. Zero-width shear zone approximations are adequate for slow slip events, but substantially overestimate the pore pressure and temperature changes during fast slip when dilatancy is included.

Segall, P. and A. M. Bradley, Slow-slip Evolves into Megathrust Earthquakes in 2D Numerical Simulations, Geophysical Research Letters. 39, L18308, doi:10.1029/2012GL052811, 2012.

Slow slip events (SSE) in many subduction zones incrementally stress the adjacent locked megathrust, suggesting that they could potentially either trigger or evolve into damaging earthquakes. We explore this with 2D quasi-dynamic simulations with rate-state friction, dilatancy, and coupled 1D pore-fluid and heat transport. Steady-state weakening friction allows transient slip to nucleate, but is inhibited by dilatant strengthening and destabilized by thermal pressurization. SSE spontaneously nucleate in Low Effective-Stress Velocity-Weakening (LESVW) regions. If the dimension of the LESVW is relatively small the SSE are trapped at its updip end, imparting a strong stress concentration in the locked zone. After several centuries SSE penetrate into the region of higher effective stress, where thermal pressurization eventually leads to dynamic rupture. For larger LESVW regions SSE tend to increase in length with time; ultimately higher slip speeds enhance thermal weakening, leading to dynamic instability within the SSE zone. In both cases the onset of the ultimate SSE is essentially indistinguishable from preceding events.

Comparison between dilatant strengthening and v -cutoff models. We found that spring-slider simulations comparing v -cutoff models with dilatancy strengthening, adjusted to the

same maximum slip-speed, can exhibit significant differences. However, these models behave very similarly in 2D continuum calculations. Fig. 1 shows space-time plots of slip speed and phase plots for a point 1/4 of the way along the fault. The model responses are qualitatively the same. We observe generally that as W/L_c increases (W = fault width, L_c = critical nucleation dimension), slip behavior for the dilatancy model is more complex than for the v -cutoff case, but local mechanical behavior remains very similar.

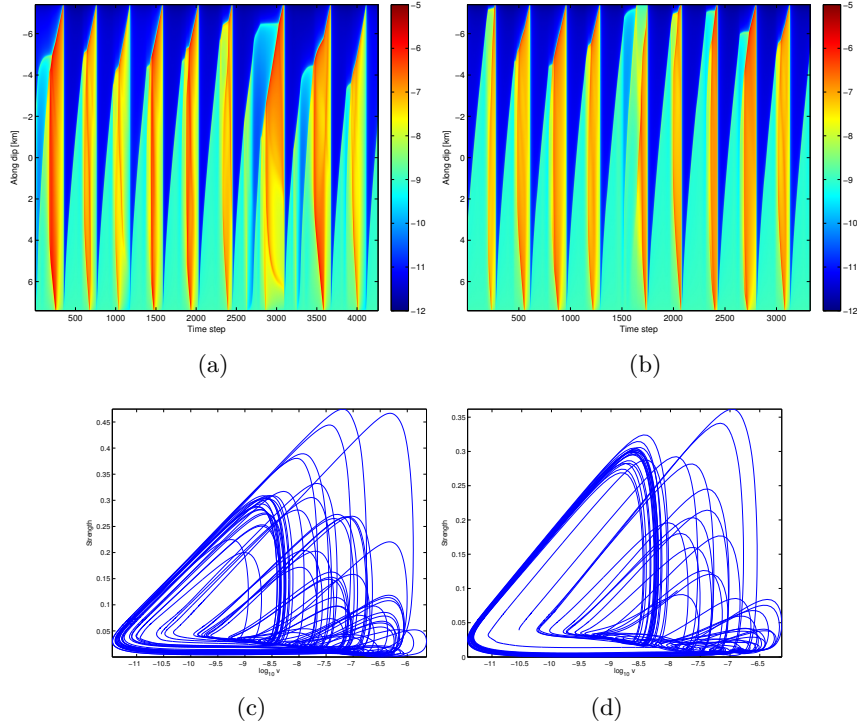


Figure 1: **(a,b)** Space-time plots of \log_{10} slip speed (color scale) for dilatancy (a) and v -cutoff (b) models. **(c,d)** \log_{10} vs fault strength phase plots for dilatancy (c) and v -cutoff (d) models. $W/L_c = 20$.

In Segall and Bradley [2012] we found that slip in the model ETS zone does not keep up with plate motion when averaged over numerous slow-slip cycles. If the ETS region accumulates a slip deficit, then it must either rupture dynamically or undergo postseismic slip. A generic feature of models we have studied to date is that the ETS region ruptures dynamically. We confirmed that this is not a property of just dilatancy models, or those with thermal pressurization, by recreating the isothermal v -cutoff simulation of Shibazaki and Shimamoto [2007]. We found that dynamic rupture of the ETS zone occurs in that and variations on that model (Fig. 2). This may seem puzzling until one considers that the increase in friction within the ETS zone at high slip

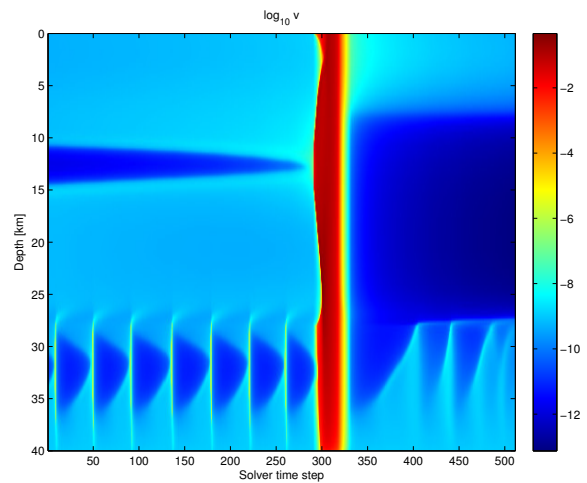


Figure 2: $\log_{10}(v)$ around the time of the main shock in the model of Shibazaki and Shimamoto [2007]. ETS region at $\sim 28 - 40$ km depth.

speed is relatively small *and* is multiplied by

a low effective stress. Thus, the small stress increase in the ETS zone cannot compensate for the large stress drop up-dip of the ETS zone. The large stress drop liberates sufficient elastic strain energy to drive ruptures a considerable distance into the velocity strengthening region.

The 1944 and 1946 earthquakes in Nankai appear to have ruptured only up-dip of the ETS zone [Dragert et al., 2004]. This has lead many to conclude that the ETS zone in Cascadia does not rupture dynamically. The fault physics that would allow this remain unclear. As a preliminary test, we experimented by moving the transition in the weakening-to-strengthening parameter v_2 to shallower depth (by 6 km), into the region of higher effective normal stress, $\bar{\sigma}$, thereby amplifying the velocity dependent increase in friction. This resulted in the slip-speed in the ETS zone during the mainshock decreasing by 1 to 2 orders of magnitude. Thus, it would appear that some models may allow predominantly afterslip in the ETS zone, although more work needs to be done to see if this can be made consistent with the observations in Nankai.

Improved numerical methods, including extension to 3D. Simulation of ETS events involves combining the equations of elasticity with appropriate fault constitutive laws. Slip rate is determined by friction and tractions acting on faults. Each fault is discretized into N elements. Each component of slip $s^{(i)}$ and traction $\tau^{(j)}$ is related by a matrix-vector product (MVP) $\tau^{(j)} = B^{(ij)}s^{(i)}$. We drop the superscripts and focus on a single $N \times N$ matrix B . B is numerically dense, thus storage and time to compute an exact MVP is $O(N^2)$. In practice, N is determined by the need to resolve the smallest relevant spatial scales. In our simulations $Gd_c/b(\sigma - p^\infty)$, controls the shape of the rupture front. For laboratory values of d_c , N^2 can become prohibitively large. For this reason we have invested significant effort into developing numerically efficient methods for quasi-dynamic simulation. All of our software is open source and will greatly benefit modelers investigating general earthquake simulations, not just SSE.

H-matrices. There are a number of algorithms that form an approximation to B , denote this \bar{B} . For this application it is advantageous to use *H-matrix compression* [Bebendorf, 2008], which approximates off-diagonal blocks of B by low-rank outer products: an $m_i \times n_i$ block $B_i \approx U_i V_i^T$, where U_i has $r_i \ll \min\{m_i, n_i\}$ columns. The storage for the block is $O(r_i(m_i + n_i))$. An MVP $B_i x$ is implemented as $U_i(V_i^T x)$, which requires $O(r_i(m_i + n_i))$ work.

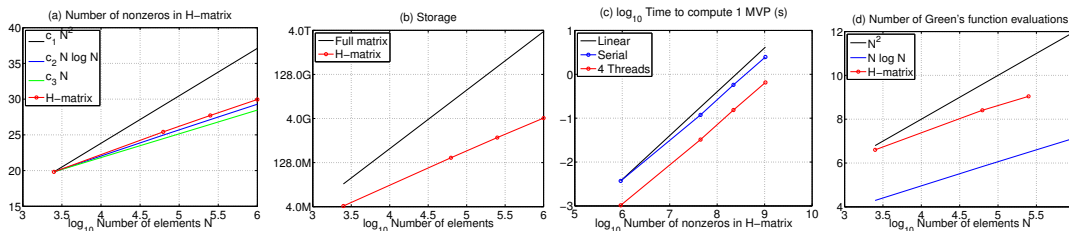


Figure 3: Plots characterizing `hmv` performance on the application in Johnson et al. [2013]. For reference, N^2 , $N \log N$, and N are shown. All axes are log₁₀. $\varepsilon = 10^{-5}$.

Let ε specify the maximum allowed Frobenius-norm-wise relative error of the approximation \bar{B} to B , and $E \equiv B - \bar{B}$. Our software library `hmv` [Bradley, 2011] forms and computes H-matrix MVP, such that \bar{B} satisfies $\|E\|_F \leq \varepsilon \|B\|_F$. This implies a useful error bound on a MVP: $\|Bx - \bar{B}x\|_2 \leq \varepsilon \|B\|_F \|x\|_2$. We characterize the performance of `hmv` using the application described in Johnson et al. [2013]. A planar fault is discretized into $N \approx 10^6$ uniform elements. Figure 3(a) shows the number of nonzero elements (nnz) in \bar{B} as a function of N ; both storage and the work to compute an MVP are $O(\text{nnz})$. Storage grows as $N \log N$ for large N . Figure 3(b) shows the storage required (single precision) for \bar{B} . For $N = 10^6$, B

requires 3.6 TB while \bar{B} requires ~ 4 GB. Figure 3(c) shows the time to compute one MVP. Ideal growth is linear in nnz , and in practice it is indeed linear. Figure (d) shows the number of Green’s function evaluations in forming the H -matrix as a function of array size. The number scales roughly linearly in N rather than as N^2 . `hmmvvp` is now independent of MATLAB, though it has a MATLAB interface. `hmmvvp` already had OpenMP and MPI-parallelized MVP routines. Recently, we implemented the compression procedure in C++ and provide versions parallelized by OpenMP and MPI. On our 16-core computer, compression is approximately 20 times faster than the MATLAB version.

What is the downdip limit of megathrust events and how does this relate to the depth distribution of ETS events?

We continued to study this problem via a combination of modeling and comparison to geodetic data. A robust result of our simulations is that ETS slip does not keep up with plate motion. When averaged over many ETS cycles, the shear stress within the ETS zone remains nearly constant. This requires slip deficit to accumulate within the ETS zone [Segall and Bradley, 2012] and (Figure 4). Some geodetic inversions place the downdip limit of locking near the coastline, at depths on the plate interface of ~ 20 km [Flück et al., 1997], leaving a gap between the locked zone and the top of the ETS zone. Others have found that partial coupling extends nearer to the top of the ETS zone [Chapman and Melbourne, 2009, McCaffrey, 2009].

If the ETS zone accumulates slip deficit, then it must either rupture dynamically or undergo postseismic slip. A generic feature of models we have studied to date is that the ETS region ruptures dynamically. This is also a property of isothermal v -cutoff simulations (see above). The increase in friction within the ETS zone at high slip speed is relatively small *and* is multiplied by a low effective stress. Thus, the small stress increase in the ETS zone cannot stop the rupture.

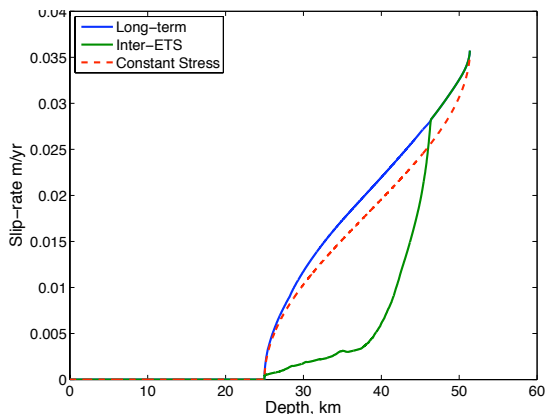


Figure 4: Inter-ETS and “Long-term” slip-rate (averaged over many SSE); “Constant Stress” analytical result for fault locked from $z < 25$ km, slipping at constant shear stress for $25 < z < 51$ km.

weakening (LESVW) region is at roughly the correct depth, which also generally coincides with the depth extent of tremor.

We next compared predicted inter-ETS slip-rates and long-term slip-rates (averaged over many ETS) for a generic dilatancy strengthening model to the corresponding GPS velocities. In both cases we find that model over-predicts velocity at coastal stations. This implies that the physics based model has too much shallow locking. It is possible for stable sliding to occur up-dip of the ETS zone even with velocity weakening friction. However, this requires the local

We explored how predictions of physics based models compare to GPS results in the Olympic Peninsula - southern Vancouver Island region. We determine the mean ETS displacement and inter-ETS velocity at 29 stations with data from 2002-2010, and compare with model predictions, using a pseudo-3D approach. The plate interface is tessellated with triangular dislocations. Slip at each point on the fault is taken from the 2D physical model at the corresponding depth. Since the physics-based model is 2D, we taper ETS slip along-strike. The fit to the mean ETS displacements is remarkably good (Figure 5). The model also fits the sign of the vertical displacements at over 80% of the stations. This suggests that the low effective stress, velocity

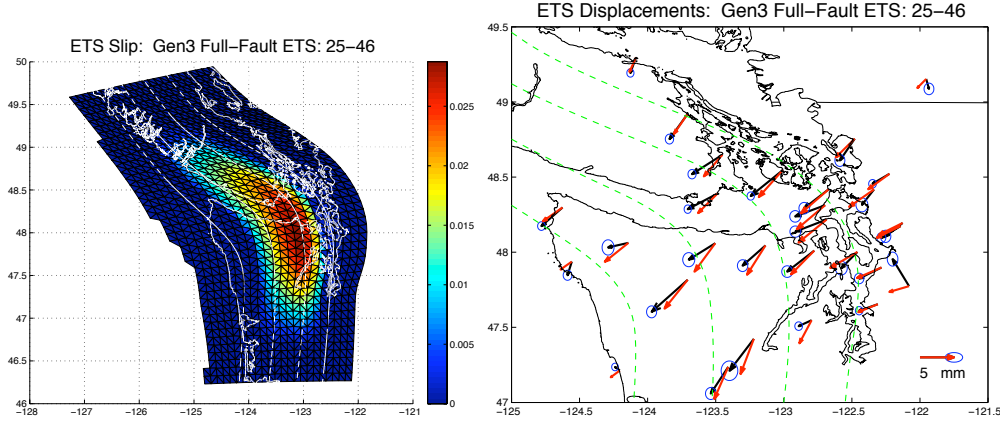


Figure 5: a) Mean model SSE slip, tapered along strike. b) Mean observed (black with 95% confidence ellipses) and model (red) ETS displacements. Contours at 20, 30, 40, and 50 km.

L_c to be large, implying either nearly velocity neutral friction, or large d_c .

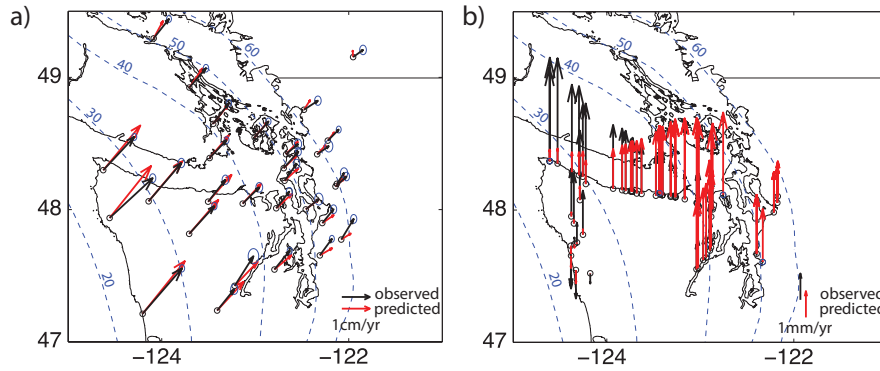


Figure 6: Predicted and observed interseismic velocities (a) horizontal and (b) vertical) for elastic half-space models with constant shear stress transition zone spanning 22-45 km depth.

Most analyses of interseismic deformation assume fully elastic response, however it is well known that if the Maxwell relaxation time t_R is short compared to the earthquake cycle time T_{cyc} , that viscoelastic relaxation alters the deformation field [e.g. Wang et al., 2012, Segall, 2010, Chapter 10]. We studied this using viscoelastic cycle models with imposed periodic earthquakes [Johnson and Fukuda, 2010, Segall, 2010].

We simplify the problem by applying the analytical slip-rate distribution for an elastic half-space driven by constant v^∞ below depth Z_l , locked above Z_u , and creeping at constant shear stress in between (dashed curve in Fig. 4). We then estimate Z_l , Z_u , the elastic layer thickness (H), and Maxwell relaxation time t_R (4 parameters total) from the data.

We investigated this [Kim et al., 2012] with Ph.D. student Marina Kim. Ray Weldon generously provided vertical rates from leveling and tide-gauges, that we combine with horizontal GPS velocities. For an elastic model with ETS (constant stress) zone between 25 and 40 km depth the fit to the GPS velocities is reasonable, however, the fit to the vertical rates is poor (Figure 6). Figure 7 shows misfit surfaces for *viscoelastic models* with $t_R=60$ and $H = 45$ km. The middle panel shows the fit to the horizontal GPS velocities. The optimal model is $Z_u \sim 15$ km and $Z_l \sim 40$ km. The depth of complete locking Z_u could exceed 15 km, but only if Z_l is

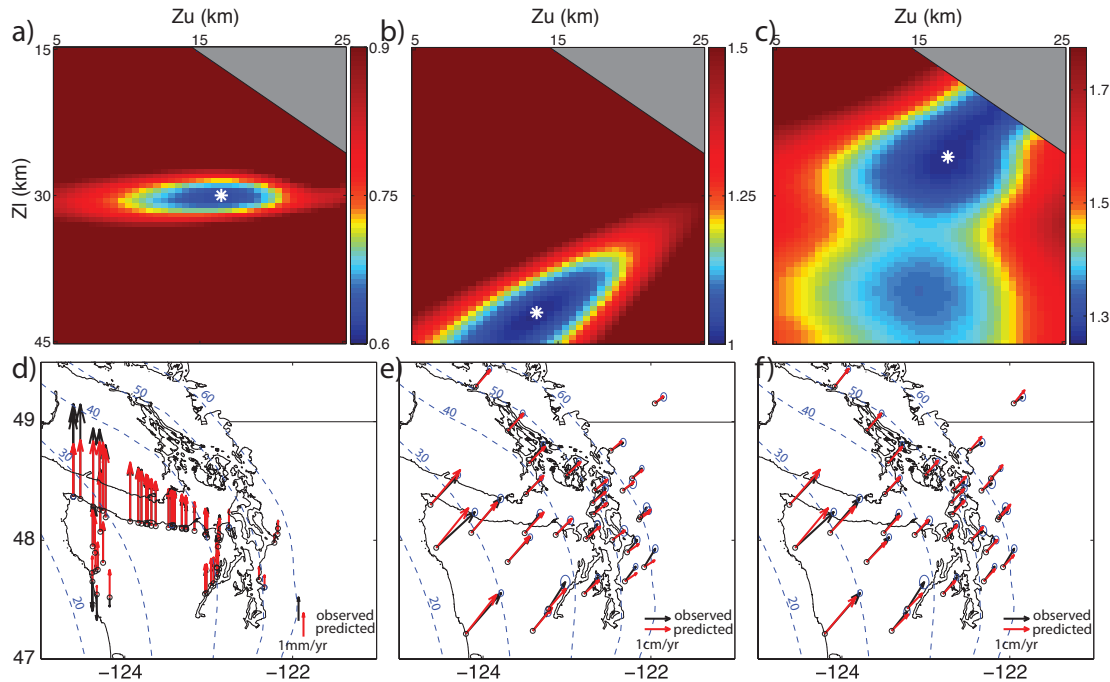


Figure 7: Results for $t_R = 60$ and $H=45$: a-c) Root mean square of residuals over ranges of Z_u and Z_l for vertical; horizontal velocity; and horizontal baseline rates. White star is the best fitting model. d-f) Observed (black) and predicted (red) data corresponding to the white star in 3(a)-3(c).

shallower than the bottom of the ETS zone.

We restricted attention to the Olympic Peninsula - Vancouver Island area to minimize effects of forearc rotation, however since we model absolute velocities we are not immune to such biases. Since baseline length changes are invariant to rigid body motions, we also generated a linearly independent set of baselines invariant to rigid-body motions, using a QR factorization approach that keeps the mapping from velocities to baselines as well conditioned as possible. The right panel in Figure 7 shows fitting baseline rates changes the interpretation; the best fit is locked to about 17 km with creep at constant stress to a depth of ~ 25 km. There is a secondary minimum in the misfit surface with creep to a depth closer to 40 km. However, the vertical rates (left panel) strongly constrains Z_l to roughly 30 km. Fitting baseline rates does allow better overlap of the acceptable depth parameters to the vertical data than fitting horizontal velocities.

A plausible, but imperfect, fit to both the vertical and horizontal data can be found with a fault that is fully locked to a depth of 16 km and transitions to creep at the full plate-rate at a depth of ~ 30 km (Figure 8). The conclusion of this analysis is that viscoelastic effects make a difference, but cannot explain the discrepancy between the data (particularly the vertical) and a model that is fully locked to the top of ETS zone. This implies that there must be steady creep at shallower depth above the ETS zone, although the mechanical basis for this is unknown.

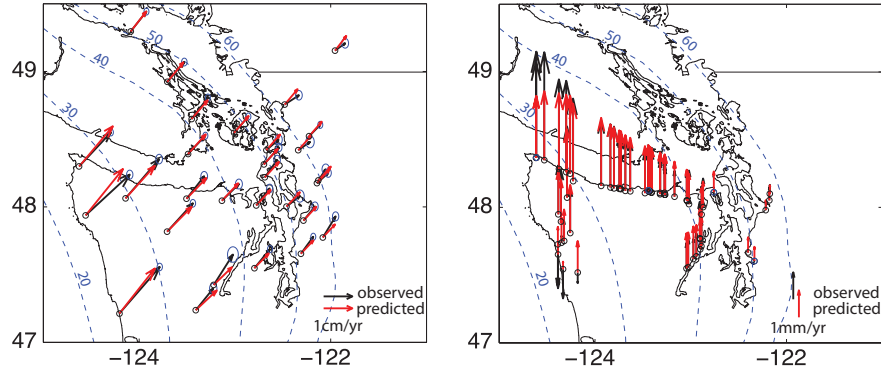


Figure 8: Example of a set of parameters fitting both horizontal and vertical components: $t_R = 50$, $H = 42.5$, $Z_u = 16$, $Z_l = 29.5$. Vertical data is highly sensitive to the slip distribution.

2 Bibliography supported by this grant, exclusive of abstracts

1. A. M. Bradley. H-Matrix and block error tolerances. Technical Report arXiv:1110.2807v1 [math.NA], 2011.
2. Noel M. Bartlow, Shin'ichi Miyazaki, Andrew M. Bradley, and Paul Segall. Space-time correlation of slip and tremor during the 2009 cascadia slow slip event. *Geophys. Res. Lett.*, 38(18):L18309–, September 2011. ISSN 0094-8276.
3. P. Segall and A. M. Bradley. Slow vs fast slip due to competition between thermal pressurization and dilatant strengthening. *J. Appl. Mech.*, 79:doi:10.1115/1.4005896., 2012a.
4. P. Segall and A. M. Bradley. Slow-slip triggering of dynamic rupture in 2d numerical simulations. *Geophysical Research Letters*, 39(18):L18308, 2012b.

References

- M. Bebendorf. *Hierarchical Matrices: A Means to Efficiently Solve Elliptic Boundary Value Problems*. Springer, 2008.
- A. M. Bradley. H-Matrix and block error tolerances. Technical Report arXiv:1110.2807v1 [math.NA], 2011.
- J.S. Chapman and T.I. Melbourne. Future Cascadia megathrust rupture delineated by episodic tremor and slip. *Geophysical Research Letters*, 36(22):L22301, 2009.
- H. Dragert, K. Wang, and G. Rogers. Geodetic and seismic signatures of episodic tremor and slip in the northern Cascadia subduction zone. *Earth, Planets, and Space*, 56(12):1143–1150, 2004.
- P. Flück, R. D. Hyndman, and K. Wang. Three-dimensional dislocation model for great earthquakes of the Cascadia subduction zone. *J. Geophys. Res.*, 102:20539–20550, 1997.
- J K. M. Johnson and J. Fukuda. New methods for estimating the spatial distribution of locked asperities and stress-driven interseismic creep on faults with application to the San Francisco Bay Area, California. *J. Geophys. Res.*, 115:B12408, 2010. doi: 10.1029/2010JB007703.
- K. M. Johnson, D. Shelly, and A. M. Bradley. Numerical simulations of tremor-related creep reveal weak lower-crustal root of the San Andreas fault. *Geophys. Res. Lett.*, 40:1300–1305, 2013. doi: 10.1002/grl.50216.
- M. J. Kim, P. Segall, and K. M. Johnson. Constraining interseismic deformation in the cascadia subduction zone using a viscoelastic earthquake cycle model. In *Eos Trans. AGU, Fall Meet. Suppl., Abstract G43B-0926*, 2012.
- R. McCaffrey. Time-dependent inversion of three-component continuous gps for steady and transient sources in northern Cascadia. *Geophys. Res. Lett.*, 36:L07304, 2009.
- Y. Okada. Internal deformation due to shear and tensile faults in a half-space. *Bull. Seism. Soc. Am.*, 82, 1992.
- P. Segall. *Earthquake and Volcano Deformation*. Princeton Univ. Press, 2010.
- P. Segall and A. M. Bradley. Slow-slip evolves into megathrust earthquakes in 2d numerical simulations. *Geophysical Research Letters*, 39(18):L18308, 2012. doi: 10.1029/2012GL052811.
- B. Shibazaki and T. Shimamoto. Modeling of short-interval silent slip events in deeper subduction interfaces considering the frictional properties at the unstable-stable transition regime. *Geophys. J. Intl.*, 171:191–205, 2007.
- K. Wang, Y. Hu, and J. He. Deformation cycles of subduction earthquakes in a viscoelastic earth. *Nature*, 484(7394):327–332, 2012.